arXiv:cond-mat/0309313v1 [cond-mat.supr-con] 12 Sep 2003

Proximity and Josephson effects in superconductor - antiferromagnetic Nb / γ-$Fe_{50}Mn_{50}$ heterostructures

C. Bell, E. J. Tarte, G. Burnell, C. W. Leung, D.-J. Kang, M. G. Blamire
Materials Science Department,
IRC in Superconductivity and IRC in Nanotechnology,
University of Cambridge, United Kingdom
(Dated: February 2, 2008)

We study the proximity effect in superconductor (S), antiferromagnetic (AF) bilayers, and report the fabrication and measurement of the first trilayer S/AF/S Josephson junctions. The disordered f.c.c. alloy γ-$Fe_{50}Mn_{50}$ was used as the AF, and the S is Nb. Micron and sub-micron scale junctions were measured, and the scaling of $J_C(d_{AF})$ gives a coherence length in the AF of 2.4 nm, which correlates with the coherence length due to suppression of T_C in the bilayer samples. The diffusion constant for FeMn was found to be 1.7×10^{-4} m^2s^{-1}, and the density of states at the Fermi level was also obtained. An exchange biased FeMn/Co bilayer confirms the AF nature of the FeMn in this thickness regime.

PACS numbers: 74.45.+c 75.50.Ee 85.25.Cp 85.70.Kh
Keywords: Josephson junction, antiferromagnet, proximity effect, exchange bias

I. INTRODUCTION

From the earlist work of Hauser et al [1] there has been considerable interest in the proximity effect between thin film superconductors (S) with both ferromagnetic (F) and antiferromagnetic (AF) materials. More recently Nb/Cr multilayers [2], Nb/CuMn (spin-glass) systems have been studied [3], as have Cr/V/Cr trilayers [4]. The recently renewed interest in the S/F proximity effect due to the oscillating order parameter in the F layer and the so-called π-shift, recently found experimentally [5, 6], has not led to complimentary experiments in S/AF heterostructures. As has been pointed out by Krivoruchko [7], the nesting features of Fermi surfaces of the so-called band-antiferromagnets destroys the symmetry in momentum space, similar to the splitting of the Fermi surface in the F case. Therefore a band AF heavily suppresses superconductivity, but without the oscillating order parameter found in the F case which is necessary to realise π-junctions.

There has been much theoretical literature concerning S/F heterostructures (bilayer, trilayers, and multilayers: for a review see [8]). The various effects on the superconducting critical temperature, field and current density, (T_C, H_C and J_C), of the parallel and anti-parallel configurations of the F layers is of great interest. Various theoretical predictions have been made for J_C enhancement in the case of S/F/X/F/S Josephson junctions, when the F layers have their moments switched from parallel to anti-parallel, with large effects for X = insulator (I),[9, 10, 11], more weakly in the case of X = normal (dirty) metal (N) [12]. Spin torque on the F layers due to the Josephson current has been predicted for X = N [13]. To achieve these 'spin-active' junctions, techniques can be borrowed from the magnetics community in the fabrication of spin-valve devices. In these cases the anti-parallel alignment is achieved either by the use of two materials with different coercive fields, or by using an AF to 'pin' (exchange bias) one of two otherwise identical F layers. In the latter case this can be done by field cooling through the blocking temperature (which is $\leq T_N$, the Néel temperature), which increases the coercive field, and shifts the centre of the magnetic hysteresis loop to a non-zero applied field. The latter technique was used in the F/S/F trilayers studied in [14]. If this technique is to be applied to the case of S/F/X/F/S Josephson junctions, it is crucial to understand the Josephson effect through an AF, as the device is built up layer by layer.

The effect of magnetic and non-magnetic impurities in the barriers of S/N/S junctions has been previously studied - including the spin glasses CuMn, and AgMn [15, 16], and CuNi [17]. In these cases the barrier thicknesses were of the order of 100 nm or thicker, (since the impurity concentrations were relatively small: for example a maximum of 4.6 at.% Mn in the case of CuMn in [16]). To our knowledge no measurements have ever been made of AF Josephson junctions and, in particular, with the AF γ-$Fe_{50}Mn_{50}$. In this paper we present bilayer T_C measurements of the proximity effect between FeMn and Nb, and the first measurement of the Josephson effect through an AF. These measurements enable the coherence length in the AF to be found, and hence the diffusion constant, and in addition, the density of states at the Fermi level of the FeMn to be calculated.

II. EXPERIMENTAL DETAILS

All films were deposited on (100) oxidised silicon substrates by d.c. magnetron sputtering at 0.5 Pa, in an in-plane magnetic field $\mu_0 H \sim 40$ mT. The sputtering system was cooled with liquid nitrogen and had a base pressure better than 3×10^{-9} mbar. The system was fitted with a load lock, which minimizes run to run variation by keeping the targets under constant vacuum. Deposition rates were of the order of 0.08 nm/s for the Cu, Co

and FeMn targets, and 0.03 nm/s for Nb. Film thicknesses were controlled by varying the exposure time under the magnetron targets. For all samples containing FeMn, a 5 nm underlayer of Cu was grown, in order to achieve the required f.c.c. AF γ-FeMn phase [18].

For the trilayer devices, a Nb/Cu/FeMn/Nb sandwich was grown *in situ*; FeMn thickness, d_{FeMn} was in the range $2-6$ nm, both Nb thicknesses were 150 nm. The films were patterned to micron scale wires with broad beam Ar ion milling (1 mAcm^{-2}, 500 V), and then processed with a Ga focused ion beam to achieve vertical transport with a device area in the range 0.25 μm^2 - 1.2 μm^2. The fabrication process is described in detail elsewhere [19]. For the bilayer measurements Cu/FeMn/Nb films were grown.

All transport measurements were made in a liquid He dip probe. The critical current (I_C) and normal state resistance (R_N) were measured with room temperature electronics. For devices with a $I_C R_N > 1$ μV a current-voltage ($I-V$) characteristic was directly measured. For samples with $I_C R_N < 1$ μV a differential resistance measurement was made with a lock-in amplifier, and the I_C was found as a peak in the dV/dI measurement. For the T_C measurements a four-point configuration was used on unpatterned 5×10 mm films. The rate of cooling was $< 10^{-2}$ K/s near T_C.

III. RESULTS

In this Section the results of T_C measurements on AF/S bilayers are presented, followed by the measurements of S/AF/S Josephson junctions.

A. Measurements of T_C in Bilayers

Following Hübener et al [4] we have measured the film T_C independently varying the S and AF thicknesses, as shown in Figs 1 and 2 respectively. The $R(T)$ curves, showed a transition width of the order of 0.1 K, and the T_C is defined as the midpoint of the transition. An absolute error of 0.05 K was found by measuring the T_C of a thick Nb film, and repeated T_C measurements show a relative error of ~ 0.05 K. For thicknesses of FeMn < 1 nm a broadened transition (~ 0.2 K), is observed - presumably associated with large percentage variation of the film thickness over the substrate, and no consistent data was obtained in this thickness regime.

For a constant $d_{\mathrm{FeMn}} = 6.5$ nm, with varying Nb thickness, a suppression of T_C was observed relative to the plain Nb film . In Fig. 1 the final point with $T_C < 4.2$ K was measured in a closed cycle He-3 cryostat, with a different calibration and thermal environment, hence the relative error in T_C is larger. For a constant Nb thickness of 25 nm the T_C of the film drops dramatically as soon as the thinnest layer of FeMn is grown underneath, (the two points at $d_{AF} = 0$ in Fig. 2 are for Nb only and a Nb/Cu bilayer respectively). This implies a short coherence length ξ_{AF} in the FeMn- which we will show correlates with the results from the Josephson junctions. As a comparison, measurements on plain Nb films of decreasing thickness were also made, since in this thickness regime, the Nb only film T_C is also decreasing, (circles in Fig. 1). The reduction can be attributed to a combination of grain size and resistivity effects, as well as the proximity effect [20]. The correlation between T_C and resistance ratio R(295 K)/R(10 K), (RRR) shown in Fig. 3 is associated with the grain size effect, and is consistent with previous studies [21].

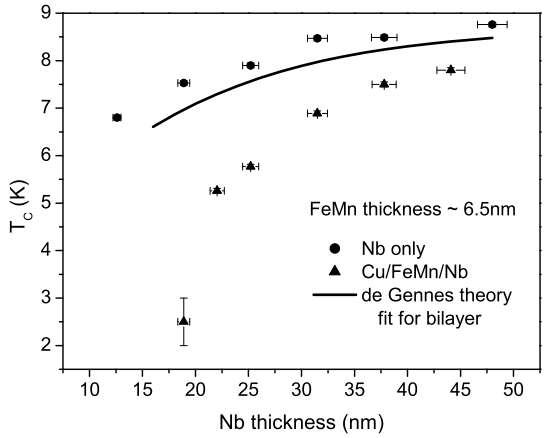

FIG. 1: Variation of T_C vs Nb thickness for a constant FeMn thickness of 6.5 nm, (triangles), compared to plain Nb films (circles). Fit to triangles is de Gennes theory (see Discussion).

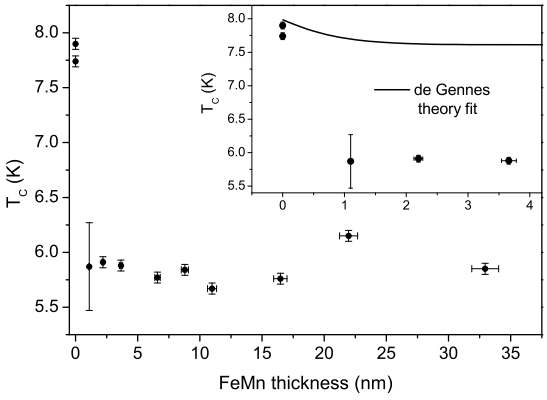

FIG. 2: Variation of T_C vs FeMn thickness for a constant Nb thickness of 25 nm. Inset: detail for thinner films, with de Gennes theory fit, (see Discussion).

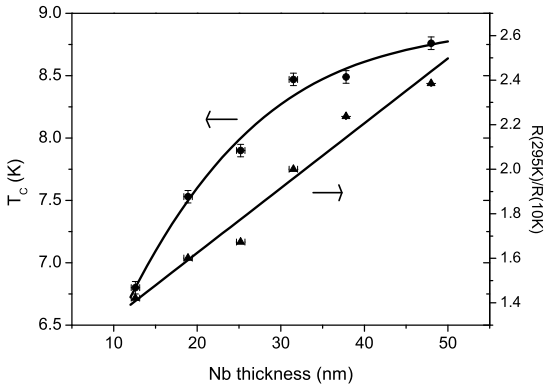

FIG. 3: T_C and RRR variation vs thickness for Nb only films. Lines are the best fit cubic and linear curves for T_C and RRR respectively.

B. Josephson junctions

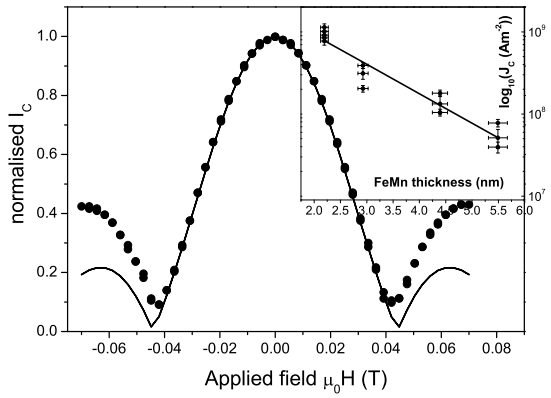

FIG. 4: Critical current modulation with an applied magnetic field, normalised to the zero field I_C. Line is a best-fit Fraunhofer pattern. Inset: Critical current density vs FeMn thickness for junctions at 4.2 K. Line is a best fit exponential $\exp(-2d_{AF}/\xi_{AF})$ with $\xi_{AF} = 2.4$ nm

The Josephson junctions showed resistively shunted junction (RSJ), $I-V$ characteristics, with I_C in the range 10 μA to 1.2 mA, and $R_N \leq 2$ mΩ. The re-entrant $I_C(H)$ in Fig. 4 shows the presence of a Josephson current through the FeMn, although we do not obtain an ideal Fraunhofer pattern. In this case the modulation is normalised to zero field critical current $I_C = 500$ μA. The junction dimension perpendicular to the direction of the applied field was ~ 600 nm and the total barrier thickness, (Cu and FeMn) was 7 nm. Correcting for the finite thickness of the Nb electrodes [22], (each is 150 nm thick), we obtain from the Fraunhofer fit a magnetic penetration depth of 40 nm. A voltage criterion is used to extract the I_C, hence the non-zero I_C is an artifact of this process: the I_C is suppressed to zero to within the 1 μV noise level of the measurement. We can estimate the Josephson penetration depth using $\lambda_J = (\hbar/2e\mu_0 J_C d)^{1/2}$. For the thinnest case with $d_{AF} \sim 3$ nm we have $J_C \sim 1\times10^9$ Am^{-2} we find $\lambda_J \sim 2$ μm, whereas the largest junction dimension is 1.2 μm, so we are close to long junction behaviour only for the largest junction with the thinnest barriers.

The inset of Fig. 4 shows the variation of critical current density, J_C, with d_{FeMn}. Assuming a dirty S/N/S junction $J_C \propto \exp(-k_{AF}d_{AF})$ [23]. Using $k_{AF} = 2/\xi_{AF}$ (see Discussion) and fitting this to the inset of figure 4, we find the characteristic decay length $\xi_{AF} = 2.4$ nm. The errors in $J_C(d)$ consist of measurement error of the sub-micron junction area, as well as scatter due to variation of d_{AF} over the area of the chip, (this is also the case for the scatter in the $I_C R_N$ data of junctions with nominally the same thickness of FeMn). There may also be additional variation due to domain structures in the AF, and spin compensation at the interfaces which are spatially inhomogeneous. All devices for a given film thickness are patterned on the same 10 mm $\times$ 5 mm chip, hence interface transparency and contamination should be comparable for a given d_{AF}.

IV. DISCUSSION

γ-$Fe_{50}Mn_{50}$, (FeMn) is an example of a f.c.c. disordered AF, and is one of the most studied materials used to exchange bias ferromagnetic films [24]. Although its magnetic / exchange bias properties have been intensively studied, the crystal structure is complex and difficult to probe, hence the precise nature of the magnetic structure of this material is still under debate [25, 26]. The electronic properties are less well studied, and the authors are not aware of any experimental studies of properties such as the Fermi velocity, electronic heat capacity, or mean free path of FeMn thin films. In this Section we use the measurements above to calculate some of the properties of the FeMn, and use them to fit the bilayer T_C measurements.

If we consider FeMn as a band antiferromagnet the coherence length in the AF is given by (in the dirty limit):

$$\xi_{AF} = \left[\frac{2\hbar D}{H_{Ex}}\right]^{\frac{1}{2}} \tag{1}$$

where $D = \frac{1}{3}v_{Fermi}\ell$ is the diffusion constant, and $H_{Ex} \sim k_B T_N$ the exchange coupling between the AF spins, similar to the exchange field in the ferromagnetic case. The additional factor of 2 compared to the F case ($\xi_F = (4\hbar D/H_{Ex})^{1/2}$) arises since the AF wave vector has the form $k_{AF} = 2/\xi_{AF}$ rather than the complex form $k_F = 2(1+i)/\xi_F$ which gives rise to the oscillating order parameter in the F case [7]. Hence, ξ_{AF} scales with

the bulk T_N, which in the case studied here is in the range $450 - 490$ K [24]. In the case of FeMn, however, because it is a highly disordered alloy system, we expect a very short mean free path ℓ, of the order of 1 nm or less [27]. Hence, a reasonable value of ξ_{AF} using equation (1) with a Fermi velocity $v_{fermi} = 2 \times 10^6$ ms^{-1} (both Fe and Mn have $v_{Fermi} \sim 2 \times 10^6$ ms^{-1}) is of the order of $4 - 5$ nm. This is in agreement with the value from the trilayer junctions, and much shorter than the corresponding coherence length in a normal metal. Further information can be gained from this measurement of the coherence length. From equation (1) using $T_N = 450$ K, and $\xi_{AF} = 2.4$ nm, the diffusion constant D is found to be 1.7×10^{-4} m^{2}s^{-1}.

Given the value of the diffusion constant D_{AF} it is possible to calculate the density of states at the Fermi level using the Einstein relation $\sigma = 2e^2\mathcal{N}(\epsilon_F)D$, [28]. For this the value of $\sigma_{\rm FeMn}$ is required. This was found using a series of Cu(5 nm)/FeMn/Nb(6 nm) films grown for differing FeMn thicknesses (the Nb serves as a cap to prevent oxidation of the FeMn). Assuming a simple parallel resistor model, plotting the ratio of total thickness and resistivity against FeMn thickness should give a straight line with gradient equal to the conductivity of the FeMn. $\sigma_{\rm FeMn}$ is found to be $8.4 \times 10^5 (\Omega{\rm m})^{-1}$, from the linear fit (Fig. 5). Hence using $\sigma = 2e^2\mathcal{N}(\epsilon_F)D$, with the values of D and $\sigma_{\rm FeMn}$ above, the density of states at the Fermi level, $\mathcal{N}(\epsilon_F)$, in FeMn is found to be 2.7×10^{25} states J^{-1}m^{-3}. For parallel resistors, the intercept of Fig. 5 is given by $\sigma_{\rm Nb} d_{\rm Nb} + \sigma_{\rm Cu} d_{\rm Cu}$. Using the value of $\sigma_{\rm Nb}$ (see below) this intercept is predicted to be of the order of 0.16 Ω. The smaller observed value is associated with interface resistance, which would be significant for $d_{\rm Nb} = 6$ nm, which reduces the effective value of $\sigma_{\rm Nb}$. This is also consistent with a higher value of $\sigma_{\rm FeMn}$ obtained from the junction R_N values: which would also contain a component due to the interface resistance. We can now fit the

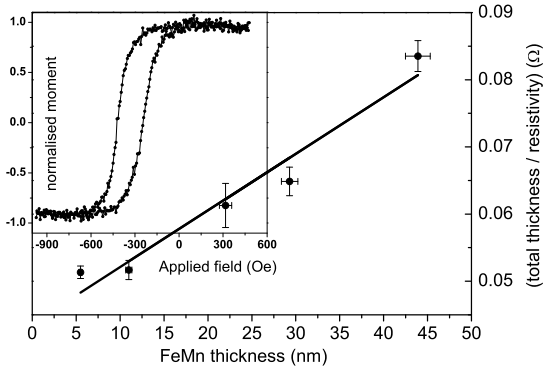

FIG. 5: Linear fit to find σ_{FeMn} using different thicknesses of FeMn in a Cu/FeMn/Nb trilayer, at 295 K. Inset: Hysteresis loop of a Nb/Cu/FeMn/Co/Nb trilayer after annealing at 0.2 T from 200 °C for 30 minutes.

bilayer T_C measurements. We do not follow reference [4] which analysed the data in terms of the Werthamer theory [29]. This considers the case that the metals are identical in the normal state - i.e. the Fermi velocities, residual resistivity and Debye temperatures are the same, and uses a single effective coherence length. However in this case the Nb and FeMn films are significantly different, and we should consider the coherence lengths of the superconductor and normal metal separately. Hence we use de Gennes theory in the one frequency approximation [23]. For the case that the normal metal film is not superconducting at any temperature - i.e. has $T_C = 0$ K we have:

$$\frac{1}{\sqrt{2}\xi_S}\sqrt{\left(\frac{T_{CS}}{T_C}-1\right)}\tan\left[\frac{d_S}{\sqrt{2}\xi_S}\sqrt{\left(\frac{T_{CS}}{T_C}-1\right)}\right] = \frac{2}{\xi_{AF}}\frac{D_{AF}\mathcal{N}_{AF}(\epsilon_F)}{D_S\mathcal{N}_S(\epsilon_F)}\tanh\left[\frac{2d_{AF}}{\xi_{AF}}\right], \quad (2)$$

where the largest root of this equation gives T_C, the transition temperature of the bilayer. Here $\mathcal{N}_{S,AF}(\epsilon_F)$ are the density of states at the Fermi level of the S and AF respectively, and T_{CS} the transition temperature of the plain S layer. All of the required parameters for equation (2) are known, or can be obtained by experiment, as we now show.

From the trilayer junctions results above we use $\xi_{AF} = 2.4$ nm. The thicknesses d_S and d_{AF} are known for a given film. To find ξ_S in the dirty limit we use $\xi_S = 0.85(\xi_0\ell)^{\frac{1}{2}}$, with $\xi_0 \approx \hbar v_{Fermi}/k_B T_0$ and substitute using the free electron form $D = \frac{1}{3}v_{Fermi}\ell = \sigma k_B^2\pi^2/3e^2\gamma$, [4, 30]. We obtain

$$\xi_S = \left[\frac{\pi\hbar k_B\sigma}{6e^2\gamma T_0}\right]^{\frac{1}{2}}. \quad (3)$$

Here the electronic specific heat capacity $\gamma = 720$ Jm^{-3}K^{-2}, [31] and $T_0 = 9.25$ K - the bulk T_C of Nb. From a van der Pauw measurement at 295 K we find a value of $\sigma_{\rm Nb} = 2.7 \times 10^7$ $(\Omega{\rm m})^{-1}$ for our films. We use a linear fit to follow the variation of RRR value with $d_{\rm Nb}$, (Fig. 3). Hence for a given thickness of Nb we calculate $\sigma_{\rm Nb}(10\ {\rm K})$, using the RRR linear fit, and then find ξ_S using equation (3). ξ_S is found to be of the order of 6 nm.

The plain Nb transition temperature T_{CS} is similarly followed using an empirical cubic fit to the T_C, as in Fig. 3. Finally from $\sigma = 2e^2\mathcal{N}(\epsilon_F)D$ the ratio $D_{AF}\mathcal{N}_{AF}(\epsilon_F)/D_S\mathcal{N}_S(\epsilon_F)$ is identical to $\sigma_{\rm FeMn}/\sigma_{\rm Nb} = 0.031$, using the above values. Hence the only remaining parameter in equation (2) is T_C, for which we solve numerically.

For varying Nb thickness, this fit with no adjustable parameters is shown as a solid line in Fig. 1, which is clearly not a good qualitative fit to the data. For the case of varying FeMn thickness, as can be seen from Fig. 2, the suppression of T_C is saturated for thicknesses >1 nm: which would be expected for a coherence length of that order. The inset of Fig. 2 shows that the theoretical fit, which saturates for $d_{AF} \geq 2.5$ nm, although the

saturation value of T_C is much higher than found experimentally. With $d_{\mathrm{FeMn}} > 10$ nm there does appear to be some additional variation of T_C, which is not expected from equation (2). However this most likely due to a different phase of FeMn being produced in films thicker than 20 nm [18]. More investigation of this behaviour is required.

A Nb(150 nm)/Cu(5 nm)/FeMn/Co/Nb(150 nm) structure was also grown as a reference to check the AF nature of the FeMn, with $d_{\mathrm{FeMn}} \sim 4.5$ nm, and $d_{\mathrm{Co}} \sim 2$ nm. $M(H)$ hysteresis loop measurements were made with a vibrating sample magnetometer, and showed that there was some exchange bias associated with the applied field during deposition. The relatively weak nature of this ($H_{bias} \sim 150$ Oe) implies that there are many misaligned domains in the Co being pinned by the AF. The film was annealed in a field of 0.2 T at 200 °C for 30 minutes, and field cooled. After annealing the exchange bias was measured as $H_{bias} \sim 335$ Oe, (Inset of Fig. 5). This shows that the FeMn is an AF in this thickness regime, as expected. Although in this regime the magnitude of the exchange bias is changing with d_{FeMn} [32], this does not imply variation of the exchange coupling energy between the spins at 4.2 K, hence we can assume a constant value of ξ_{AF}.

Many models of exchange bias in magnetic films use compensation of spins at the interface as a crucial parameter. Indeed the true structure of the present device might be S/N/F/AF/F/S: where the F layers are uncompensated AF spins. A full theoretical description of these bilayers and junctions may enable additional information concerning the nature of thin films of γ-FeMn to be gained, as well as provide a qualitative fit to the data in the present work.

V. CONCLUSIONS

We have been able to obtain the diffusion constant D, and density of states of γ-FeMn. We have also fabricated AF Josephson junctions with a coherence length $\xi_{AF} \sim 2.4$ nm. This value of ξ_{AF} was used to model AF/S bilayer T_C measurements, and with no free parameters, but gave unsatisfactory results. It is clear that a more relevant theory is required to fit the data. Although this work implies a similar strong suppression of superconductivity in AF FeMn as in the ferromagnetic case, the thicknesses used in the present work are similar to those used to fabricate spin-valves. Hence the fabrication of a Josephson spin-valve using FeMn as a pinning layer, measured below 4.2 K may possess a J_C which is not too small to be beyond experimental reach, although a AF with lower T_N, and weaker FM layers would significantly increase the J_C of the junctions.

Acknowledgments

We would like to thank Manna Ali (University of Leeds) for annealing the exchange biased film. This work is supported by the Engineering and Physical Sciences Research Council, UK.

[1] J. J. Hauser, H. C. Theuerer, and N. R. Werthamer, Phys. Rev. **142**, 118 (1966).
[2] Y. Cheng and M. B. Stearns, J. Appl. Phys. **67**, 5038 (1990).
[3] C. Attanasio, C. Coccorese, L. V. Mercaldo, M. Salvato, L. Maritato, S. L. Prischepa, C. Giannini, L. Tapfer, L. Ortega, and F. Comin, Physica C **312**, 112 (1999).
[4] M. Hübener, D. Tikhonov, I. A. Garifullin, K. Westerholt, and H. Zabel, J. Phys. Condens. Mat. **14**, 8687 (2002).
[5] V. V. Ryazanov, V. A. Oboznov, A. Y. Rusanov, A. V. Veretennikov, A. A. Golubov, and J. Aarts, Phys. Rev. Lett. **86**, 2427 (2001).
[6] T. Kontos, M. Aprili, J. Lesueur, and X. Grison, Phys. Rev. Lett. **86**, 304 (2001).
[7] V. N. Krivoruchko, Zh. Éksp. Teor. Fiz **109**, 649 (1996) , (JETP **82**, 347 (1996)).
[8] Y. A. Izyumov, Y. N. Proshin, and M. G. Khusainov, Physics-Uspekhi **45**, 109 (2002).
[9] F. S. Bergeret, A. F. Volkov, and K. B. Efetov, Phys. Rev. Lett. **84**, 3140 (2001).
[10] A. A. Golubov, M. Y. Kupriyanov, and Y. V. Fominov, JETP Lett. **75**, 190 (2002).
[11] V. N. Krivoruchko and E. Koshina, Phys. Rev. B **64**, 172511 (2001).
[12] N. M. Chtchelkatchev, W. Belzig, and C. Bruder, JETP Lett. **75**, 646 (2002).
[13] X. Waintal and P. W. Brouwer, Phys. Rev. B **65**, 054407 (2002).
[14] J. Y. Gu, C.-Y. You, J. S. Jiang, J. Pearson, Y. B. Bazaliy, and S. D. Bader, Phys. Rev. Lett. **89**, 267001 (2002).
[15] H. C. Yang and D. K. Finnemore, Phys. Rev. B **30**, 1260 (1984).
[16] J. Niemeyer and G. von Minnigerode, Z. Physik B **36**, 57 (1979).
[17] J. L. Paterson, J. Low Temp. Phys. **35**, 371 (1979).
[18] C. Tsang, N. Heiman, and K. Lee, J. Appl. Phys. **52**, 2471 (1981).
[19] C. Bell, G. Burnell, D.-J.Kang, R. H. Hadfield, M. Kappers, and M. G. Blamire, Nanotechnology **14**, 630 (2003).
[20] M. S. M. Minhaj, S. Meepagala, J. T. Chen, and L. E. Wenger, Phys. Rev. B **49**, 15235 (1994).
[21] A. Andreone, A. Cassinese, M. Iavarone, R. Vaglio, I. I. Kulik, and V. Palmieri, Phys. Rev. B **52**, 4473 (1995).
[22] M. Weihnacht, Phys. Status Solidi **32**, K169 (1969).
[23] P. G. de Gennes, Rev. Mod. Phys. **36**, 225 (1964).
[24] J. Nogués and I. K. Schuller, J. Magn. Magn. Mater. **192**, 203 (1999).
[25] G. M. Stocks, W. A. Shelton, T. C. Schulthess, B. Újfalussy, W. H. Butler, and A. Canning, J. Appl.

Phys. **91**, 7355 (2002).
[26] K. Nakamura, T. Ito, and A. J. Freeman, Phys. Rev. B **67**, 014405 (2003).
[27] P. L. Rossiter, *The Electrical Resistivity of Metals and Alloys* (Cambridge University Press, 1991).
[28] N. W. Ashcroft and N. D. Mermin, *Solid State Physics* (Holt-Saunders, 1976).
[29] N. R. Werthamer, Phys. Rev. **132**, 2440 (1963).
[30] A. B. Pippard, Rep. Prog. Phys. **23**, 176 (1960).
[31] C. Poole, *Handbook of Superconductivity* (Academic Press, 2000).
[32] R. Jungblut, R. Coehoorn, M. T. Johnson, J. aan de Stegge, and A. Reinders, J. Appl. Phys. **75**, 6659 (1994).